Journal of Proteomics 196 (2019) 162–172

Contents lists available at ScienceDirect

Journal of Proteomics

journal homepage: www.elsevier.com/locate/jprot

The C-type lectin-like receptor Nkrp1b: Structural proteomics reveals features affecting protein conformation and interactions

Lucie Hernychová[a,b,*], Michal Rosůlek[a,c], Alan Kádek[a,c,1], Václav Mareška[d], Josef Chmelík[a,c], Ljubina Adámková[a,b], Valéria Grobárová[b], Ondřej Šebesta[b], Zdeněk Kukačka[a], Kristián Skála[a], Vojtěch Spiwok[d], Jan Černý[b], Petr Novák[a,c,*]

[a] BIOCEV– Institute of Microbiology of the Czech Academy of Sciences, Vestec, Czech Republic
[b] Department of Cell Biology, Faculty of Science, Charles University, Prague, Czech Republic
[c] Department of Biochemistry, Faculty of Science, Charles University, Prague, Czech Republic
[d] Department of Biochemistry and Microbiology, University of Chemistry and Technology, Prague, Czech Republic

ARTICLE INFO

Keywords:
Structural mass spectrometry
Chemical cross-linking
Ion mobility
Homodimers
Nkrp1b
Natural killer cells

ABSTRACT

The cytotoxicity of mouse natural killer (NK) cells in response to pathological changes in target cells is regulated *via* the Nkrp1b receptor. Here, we characterized the Nkrp1b structure and structural features (stalk, loop, and oligomerization state) that affect its interactions. To study the Nkrp1b protein structure and the functional importance of its stalk, two Nkrp1b protein variants differing by the presence of the stalk were prepared. These variants were studied using a combination of structural mass spectrometry approaches with computational modeling to derive structural models. In addition, information about biological activity and localization in mammalian cells was acquired using scanning microscopy techniques and western blotting. Based on these methods, we obtained the structure of Nkrp1b ectodomain in its monomeric and dimeric conformations, identified the dimerization interface, and determined disulfide connections within the molecule. We found that Nkrp1b occurs as a mixture of monomers and homodimers, both *in vitro* and *in vivo*.

Significance: Despite the long-standing assumption that Nkrp1 proteins are homodimers connected by disulfide bonds in the stalk region, our data showed that both Nkrp1b protein variants form monomers and homodimers irrespective of the presence of the stalk. We demonstrated that the stalk is not crucial for protein dimerization or ligand binding and that Nkrp1b interacts with its natural ligands only in its monomeric conformation; therefore, dimers may have another regulatory function. Using a unique combination of computational, biochemical, and biological methods, we revealed the structural conformation and behavior of Nkrp1b in its native state. In addition, it is a first report utilizing the intermolecular chemical cross-linking of light- and heavy-labeled protein chains together with ion mobility-mass spectrometry to design the structural models of protein homodimers.

.

1. Introduction

Natural Killer (NK) cells constitute an important part of the innate immunity and act as crucial regulators of immune responses [1–5]. The key mechanism that regulates their functions is represented by a complex receptor repertoire comprising both activating and inhibitory receptors. Mouse models are often used to study NK cell biology because the mechanisms of NK cell functions are conserved among various organisms [6,7].

According to the “missing self” theory of target recognition [8], NK cells detect decreased expression or even complete absence of self-molecules, which otherwise restrict the cytotoxicity of NK cells toward healthy cells by functioning as ligands for their inhibitory receptors. Among these “health signals”, both major histocompatibility complex (MHC) class I glycoproteins and non-MHC ligands play important roles. The latter category includes host proteins regulated by the physiological state of a cell. One such molecule is the C-type lectin-related protein-b (Clr-b), a ligand of the mouse inhibitory killer cell lectin-like subfamily B member 1b (Nkrp1b/ Klrb1b) receptor [9].

The inhibitory Nkrp1b receptors are expressed on NK cells of certain

* Corresponding authors at: BIOCEV– Institute of Microbiology of the Czech Academy of Sciences, Průmyslová 595, 252 50 Vestec, Czech Republic.
E-mail addresses: lucka.hernychova@gmail.com (L. Hernychová), pnovak@biomed.cas.cz (P. Novák).
[1] Current address: Heinrich Pette Institute – Leibniz Institute for Experimental Virology, Martinistraße 52, 20,521 Hamburg, Germany

https://doi.org/10.1016/j.jprot.2018.11.007
Received 19 July 2018; Received in revised form 31 October 2018; Accepted 5 November 2018
Available online 08 November 2018
1874-3919/

mouse strains, such as BALB/c, 129S6, and SJL/J [9–12]. Their ligand, the Clr-b protein, has been observed in all tested mouse tissues except the brain [12], showing a wide expression pattern similar to that of MHC class I molecules. This naturally broad expression of Clr-b is downregulated because of tumorigenesis or viral infection [9], such as by the activity of cytomegalovirus [13] or poxvirus [14]. Furthermore, different chemotherapeutics or inducers of genotoxic and physiological stress have been shown to decrease Clr-b levels, whereas the expression of MHC class I molecules remains unchanged [15]. Thus, the Nkrp1b:Clr-b interaction pair represents a separate and independent system that regulates NK cell activity. Although it may initially seem redundant, the Nkrp1b:Clr-b system is very important as it can monitor cellular abnormalities that are not otherwise visible to cytotoxic T cells.

From a structural point of view, NK cell receptors are divided into two groups, namely immunoglobulin-like receptors and C-type lectin-like receptors (CTLRs), which include both Nkrp1b and Clr-b [16,17]. CTLRs expressed on NK cells are type II transmembrane proteins. Therefore, their C-terminal extracellular portion [the C-type lectin-like domain (CTLD)] [17], which enables interactions with binding partners, is separated from the cell surface by a stalk region. The structure of CTLDs is widely conserved among all multicellular animals [16] and comprises two α-helices, two antiparallel β-sheets, and a long loop region [18], which is the most variable and flexible part of the domain [19]. In addition, in some CTLDs, this loop participates in Ca^{2+} binding or domain-swapping dimerization [20,21]. The domain is further stabilized by two or three disulfide bridges; in fact, the four cysteines involved in the disulfide bonds are the most conserved residues within the CTLD architecture. Common disulfide bonds are Cys1-Cys4 and Cys2-Cys3, and longer forms of CTLDs can contain one additional cysteine pair located closer to the membrane and protein N-terminus [16]. The extra cysteines can create an intramolecular linkage as in the case of the CTLR NKG2D, which exists as a homodimer without any disulfide bond between its chains [22]. However, the first cysteine in the longer sequence can also bind with a corresponding cysteine in an interacting molecule and thus participate in dimerization, as previously described in CD94/NKG2 heterodimers [22]. Based on immunoprecipitation experiments, Nkrp1 receptors have been considered to be disulfide-linked homodimers for nearly three decades [23–25]. Nkrp1b contains first two cysteines of the protein sequence in the stalk; thus, this region could play a role in dimerization. In addition, the stalk can influence CTLD conformation or orientation and, consequently, ligand binding, as previously proven for the CTLR Ly49L [26].

So far, the crystal structures of Nkrp1a [27–29] and Nkrp1b [30] CTLDs (both from C57BL/6 mice) have been published. However, the Nkrp1b structure from another very popular mice strain (BALB/c) has not yet been studied in detail. It shares 85% sequence identity in the CTLD with the inhibitory Nkrp1b from C57BL/6, which appears like a very close match. However, it also displays 84% identity with Nkrp1a (C57BL/6), whose function as an activating receptor is directly contrary to that of the b isoform. Moreover, Nkrp1b (C57BL/6) is unique compared with Nkrp1b proteins from other mouse strains as it contains two additional cysteines and lacks one proline; therefore, it might fold or act very differently. On the other hand, the Nkrp1b proteins from other mice (BALB/c, SJL/J, and 129S6) are mutually highly identical (≥98%). Therefore, we believe that Nkrp1a (C57BL/6) is more relevant as a structural template for modeling the structure of unknown Nkrp1b (*e.g.*, from BALB/c) than that of Nkrp1b from the other mouse strain (C57BL/6).

Here, we propose the complete structure of native Nkrp1b (BALB/c) ectodomain, including its dimeric conformation, derived using homology modeling and a range of structural mass spectrometry (MS) techniques, namely disulfide bond mapping, intra- and intermolecular chemical cross-linking, and native ion mobility-mass spectrometry (IMMS). In addition, we highlight several important structural features (long loop and stalk regions) of Nkrp1b, which might affect the entire protein conformation, its oligomeric state, and interactions. Our functional results also demonstrated that the loop region is attached to the protein core and, therefore, does not participate in domain swapping. We further demonstrated that only Nkrp1b monomers, unlike homodimers, can interact with a ligand irrespective of the presence of the stalk region. Hence, the stalk seems unimportant for both Nkrp1b-ligand interactions and Nkrp1b dimerization, contrary to what has been considered to date.

2. Materials and methods

2.1. Nkrp1b protein sequence alignment

Amino acid sequences of the CTLDs (sequences corresponding to the residues Ser89–Ser223 according to the entire protein sequence numbering) of Nkrp1b proteins from different mouse strains (BALB/c, 129S6, SJL/J, and C57BL/6) and of Nkrp1a (C57BL/6) were aligned using Clustal Omega multiple sequence alignment tool implemented by EMBL-EBI [31].

2.2. Nkrp1b protein expression and purification

Nkrp1b from BALB/c as a whole extracellular region (Val63–Ser223) and a variant lacking the stalk region (Ser89–Ser223) were expressed in *Escherichia coli* BL-21 (DE3) cells transformed with pET-30a(+) expression vector carrying the relevant portion of the *Nkrp1b* gene. Proteins were expressed in LB medium as described previously [32]. Alternatively, isotopically labeled Nkrp1b proteins were obtained using a standard M9 minimal medium with 1 mM thiamine hydrochloride, 50μg/ml kanamycin, and $^{15}NH_4Cl$ as the only source of nitrogen.

The obtained proteins were then refolded and purified as described previously [32]. Purification involved size-exclusion chromatography using ENrich™ SEC 70 10 × 300 column from Bio-Rad (Hercules, CA, USA) with elution by a buffer containing 10 mM HEPES (pH 7.4), 150 mM NaCl, and 1 mM NaN_3. Protein concentrations in acquired fractions were determined using the spectrophotometer DeNovix DS-11 FX+ from DeNovix (Wilmington, DE, USA), and fractions were analyzed by SDS-PAGE using the Pierce™ unstained protein MW marker from Thermo Fisher Scientific (Waltham, MA, USA).

2.3. Molecular mass of the intact protein

Intact Nkrp1b protein variants (200 pmol) were desalted using a MicroTrap C4 column from Michrom BioResources (Auburn, CA, USA), eluted with 80% acetonitrile containing 0.5% formic acid, and directly measured using an electrospray ionization Fourier transform ion cyclotron resonance (ESI FT-ICR) mass spectrometer solariX XR equipped with a 15 T superconducting magnet by Bruker Daltonics (Billerica, MA, USA).

2.4. Disulfide bond mapping

Disulfide bonds were characterized as described previously [32,33]. Briefly, the procedure involved Nkrp1b separation by SDS-PAGE electrophoresis under nonreducing conditions; protein in-gel digestion using 5 ng/μl trypsin by Promega (Fitchburg, WI, USA), Asp−N, and/or GluC (both by Roche, Basel, Switzerland); peptide analysis by LC-MS using an ESI FT-ICR mass spectrometer; and finally, data processing using Data Analysis 4.1 (Bruker Daltonics, Billerica, MA, USA).

2.5. DNA cloning of msfGFP-tagged Nkrp1b

Full-length sequence of *Nkrp1b (BALB/c)* was synthesized and subcloned into pEGFPN1 vector from Shanghai Generay Biotech Co. (Shanghai, China). The *Nkrp1b* insert was then ligated into pXJ41 vector using *EcoRI* and *BamHI* (both by New England Biolabs, Ipswich,

MA, USA) restriction sites. The forward primer 5′-TCTGGATCCAATG GTGAGCAAGGGC-3′ and the reverse primer 5′-GGTCTAGATTACTTGT ACAGCTCGTCCA-3′ were used to prepare the *msfGFP* gene with *BamHI* and *XbaI* (by New England Biolabs, Ipswich, MA, USA) restriction sites. DNA fragment was then sub-cloned into the *BamHI* and *XbaI* restriction sites of pXJ41-Nkrp1b vector. The final pXJ41-Nkrp1-msfGFP vector was used for transient transfection of COS-7 cell line.

2.6. Cell cultures and transfection with pXJ41-Nkrp1-msfGFP

COS-7 cell line was grown in DMEM medium by Sigma-Aldrich (St. Louis, MO, USA) supplemented with L-glutamine and 10% fetal calf serum by Life Technologies (Carlsbad, CA, USA) at 37 °C with 5% CO_2 in a humidified incubator.

COS-7 cells were 60%–70% confluent on the day of transfection. Two million cells were transfected with 7 μg DNA (pXJ41- Nkrp1b-msfGFP) using 21 μl Lipofectamine LTX in 3 ml Opti-MEM (both by Life Technologies, Carlsbad, CA, USA). The Lipofectamine LTX complexes were incubated (30 min, room temperature) and added to cultured cells in 100 mm cell culture dishes.

2.7. Live cell imaging

COS-7 cells immobilized on poly-L-lysine-coated coverslips were imaged in a closed perfusion chamber (FCS3, Bioptechs, Butler, PA, USA) at 37 °C using a confocal laser scanning microscope FluoView 1000 with 60× water immersion, 1.2 NA objective UPLSAPO both by Olympus (Tokyo, Japan). A steady-state semiconductor laser (488 nm) was utilized for excitation. The fluorescence emission was collected using 560 nm long-pass and 460–520 nm band-pass filters.

2.8. Nkrp1b-msfGFP immunoblotting

COS-7 cells transfected with pXJ41-Nkrp1b-msfGFP were washed with phosphate buffered saline (PBS) and lysed on ice (40 min) in 100 μl lysis buffer [20 mM Tris-HCl (pH 8.2), 100 mM NaCl, 10 mM EDTA, 1% n-decyl-β-D-maltopyranoside, 50 mM NaF, 1 mM orthovanadate, 20 mM iodoacetamide, and protease inhibitor mixture from Serva (Heidelberg, Germany)]. Reducing samples were supplemented with 100 mM dithiothreitol (Serva, Heidelberg, Germany). The insoluble material was removed by short centrifugation at 3000 ×*g* for 3 min at 4 °C. Proteins were separated by SDS-PAGE in a 10% polyacrylamide gel and were then transferred onto a nitrocellulose membrane by Pall Corporation (Port Washington, NY, USA) using blotting apparatus Trans-Blot SD Semi-Dry by Bio-Rad (Hercules, CA, USA). The transfer was run at 0.80 mA/cm^2 of transfer membrane for up to 1.5 h. Proteins were detected with polyclonal anti-GFP antibody by Exbio (Vestec, Czech Republic) according to the manufacturer's instructions. As a loading control, β-actin was detected using anti-β-actin antibody by Santa Cruz (Dallas, TX, USA).

2.9. Nkrp1b protein covalent labeling

Nkrp1b protein variants were labeled with amine-reactive ATTO 590 dye from ATTO-TEC (Siegen, Germany) according to the manufacturer's protocol. In addition to the standard protocol, ethanolamine in two-molar excess of the fluorescent dye ATTO 590 was added to the samples after incubating Nkrp1b protein variants with ATTO 590 to eliminate any unbound dye. Excessive dye was then removed using Micro Bio-Spin P-6 desalting columns by Bio-Rad (Hercules, CA, USA).

2.10. Interaction of Nkrp1b-ATTO 590 with bone marrow-derived cells

Bone marrow-derived cells were isolated from the femurs of both C57BL/6 and MHC II-EGFP knock-in mice [originally derived from a 129/Sv mouse by replacing the MHC class II gene for the β-chain gene version tagged with enhanced green fluorescent protein (EGFP) and backcrossed with C57BL/6] [34]. Eight-week-old male mice were bred and housed in the animal facility at the Charles University (Prague, Czech Republic), kept under natural day/night conditions (22 °C, 55% humidity), and fed on an ST1 diet (Velaz, Prague, Czech Republic). All procedures were conducted in accordance with the European Convention for the Care and Use of Laboratory Animals as approved by the Czech Animal Care and Committee.

The mice were euthanized by overdosing the anesthetics. Cells were flushed out from the bone marrow cavity with RPMI 1640 medium without phenol red and supplemented with L-glutamine by Lonza (Basel, Switzerland), 10% fetal bovine serum by Gibco (Dublin, Ireland), 100 U/ml penicillin, and 100 μg/ml streptomycin by PAA Laboratories (Pasching, Austria). Cells were plated and cultivated on coverslips from P-LAB (Prague, Czech Republic) in 24-well plates by Schoeller Pharma (Prague, Czech Republic) for 5 days in a humidified atmosphere at 37 °C with 5% CO_2. Mouse granulocyte macrophage colony-stimulating factor (GM-CSF) was added to the cell culture during the second day of cultivation. Supernatant from hypoxanthine-aminopterin-thymidine-sensitive Ag8653 myeloma cells transfected with murine GM-CSF cDNA (isolated from a T cell clone and ligated into BCMGSNeo vector) served as a source of GM-CSF [35,36]. After 5 days of cultivation (up to 50% density), cells were washed with PBS, fixed with 3.7% paraformaldehyde in PBS (20 min, room temperature), treated with 15 mM NH_4Cl (10 min, room temperature) to reduce unspecific formaldehyde-caused antibody binding, blocked with 1% bovine serum albumin (BSA; Sigma-Aldrich, St. Louis, MO, USA) in PBS (10 min, room temperature), and stained with Nkrp1b-ATTO 590 protein forms (1 h, room temperature). Labeled protein variants were diluted with 1% BSA to three different concentrations (0.1, 0.5, and 1 μg/ml). Unstained cells served as a negative control, and lectin peanut agglutinin (PNA) from *Arachis hypogaea* (peanut) conjugated with Alexa Fluor® 568 by Thermo Fisher Scientific (Waltham, MA, USA) of the same concentrations as Nkrp1b proteins served as a positive control. After 1 h incubation with labeled proteins, cells were washed five times with PBS. Coverslips with cells were then transferred onto microscope slides from P-LAB (Prague, Czech Republic) and mounted in Fluoroshield™ with DAPI by Sigma-Aldrich (St. Louis, MO, USA).

2.11. Fluorescence microscopy (ScanR)

Images were acquired using Olympus ScanR system with Hammatsu ORCA C4742–80-12AG camera with three channels by Olympus (Tokyo, Japan). Multi-band DAFITR emission filter sets with excitation wavelength of 300–400 nm and emission wavelength of 435–479 nm for DAPI staining, 549–559 nm/600–656 nm for red Nkrp1b-ATTO 590 or Alexa Fluor® 568 fluorescence, and short-pass emission filter 460–490 nm/510–550 nm for MHC II-EGFP were used. Olympus UPLSAPO 20×/0.75 NA objective with short working distance was used for scanning. For each slide (in duplicates), 36 fields of view were acquired. Therefore, several hundreds of cells were used for statistical analyses. Only segmented particles (cells) that were smaller than 120 μm^2 and contained the nucleus were analyzed using Olympus soft imaging solutions 3.0.1. build 6074 software. Finally, the dependence of the mean fluorescence intensity on the protein concentration for each data set was plotted. The mean value, standard deviation, and standard error of the mean were calculated for each dataset.

2.12. Chemical cross-linking

The experimental setup followed previously published guidelines [37]. An equimolar mixture of non-deuterated and deuterated amine-reactive cross-linkers disuccinimidyl glutarate (DSG) and disuccinimidyl suberate (DSS), respectively (both from ProteoChem, Hurricane, UT, USA), were used. Sixteen micromolar Nkrp1b protein in 10 mM HEPES (pH 7.4) and 150 mM NaCl buffer was incubated with

20× or 50× molar excess of the cross-linking agents for 2 h. Following quenching of the reaction with two-molar excess of buffered ethanolamine, Nkrp1b protein variants were separated by SDS-PAGE in a 12% polyacrylamide gel under reducing conditions and visualized by Coomassie Brilliant Blue R-250 staining. Protein bands corresponding to monomeric and isotopically labeled dimeric Nkrp1b forms were excised, in-gel reduced using 30 mM Tris(2-carboxyethyl)phosphine (TCEP; 5 min at 60 °C), alkylated with 40 mM iodoacetamide (30 min at room temperature in the dark), and digested with trypsin in the ratio 1:20 (*w*/w) trypsin:protein (overnight at 37 °C) in 50 mM 4-ethylmorpholine buffer (pH 8.3) with 10% acetonitrile. Peptides were extracted from the gel as described previously [38], desalted using peptide MicroTrap C18 column from Michrom Bioresources (Auburn, CA, USA), and dissolved in 0.1% trifluoroacetic acid with 5% acetonitrile to a final concentration of 5 ng/μl prior to analysis.

Five picomoles of peptide mixture were injected onto an analytical reversed phase column (Zorbax 300SB-C18 3.5 μm, 0.3 × 150 mm from Agilent Technologies, Santa Clara, CA, USA) with a trap pre-column (Zorbax 300SB-C18 5 μm, 0.3 × 5 mm) and separated using a 5%–40% acetonitrile gradient over 35 min. Throughout chromatography, 0.1% formic acid was used as an ion-pairing agent. The HPLC system was directly coupled with an ESI source of an FT-ICR mass spectrometer solariX XR equipped with 15 T superconducting magnet Bruker Daltonics (Billerica, MA, USA). The mass spectrometer was operated in positive broadband mode over 250–2500 *m/z* range with 1 M data point acquisition. Data processing was performed using Data Analysis 4.4 (Bruker Daltonics, Billerica, MA, USA). All peptide signals from the entire chromatogram were exported using Snap 2.0 algorithm to the text file, which served as an input for an in-house-developed program based on the Links algorithm [39]. Using Links, possible amino acids modifications (alkylation of cysteine in case of cross-linking reactions and oxidation of methionine), specific cleavage, possibility of missed cleavages (set to 3), and modifications of relevant amino acids by cross-linking agents or disulfide bonds were considered. Only hits below the error of 2 ppm were regarded as positive. Finally, isotopic envelopes of identified peptides connected by cross-link or disulfide bond, respectively, were manually checked in MS spectra.

2.13. Nkrp1b homology modeling and molecular dynamics

Homology models of Nkrp1b were created using Modeller 9.19 software [40]. An NMR (pdb:2MTI) structure and X-ray structures (pdb:3T3A, 3M9Z) of Nkrp1a as well as an X-ray structure of human LLT1 (pdb:4QKH) and CLEC5A (pdb:2YHF) were used as templates for the homology modeling of different conformations and the monomeric and dimeric states of the Nkrp1b protein. To model the stalk region (residues Ser69–Gln79), *ab initio* modeling was performed using the Rosetta package version 2017.08.59291 with the scoring function talaris2014 [41]. The stalk sequence was submitted to Fragment Libraries service of Robetta server [42]. The resulting fragment files were used to generate 2000 models, which were analyzed by principal component analysis in the Rosetta software.

The disulfide bonds were defined according to MS experimental results. The MS-derived distances were restrained as the C^{α}–C^{α} distance with an upper bound of 20.5 Å with the standard deviation of 3.0 Å for the DSG and an upper bound of 24.2 Å with the standard deviation of 3.0 Å for the DSS.

A total of 50 homology models of each Nkrp1b variant were generated and subsequently assessed by the Modeller objective function, Discrete Optimized Protein Energy profiles [43], and global distance test [44,45]. Further, the best 10 models were subjected to quality assessments using experimentally measured collision cross-section of the Nkrp1b molecules.

Selected homology models of Nkrp1b protein variants were subjected to molecular dynamics simulations using Gromacs 5.1.4 [46] with AMBER99SB-ILDN force field. Each Nkrp1b model was centered in the cubic box, at least 1 nm from its edge. The box contained TIP3 water molecules and four Na^+ atoms (eight atoms in case of dimeric Nkrp1b) to neutralize the charge of the system. Each Nkrp1b model was relaxed by 160,000–190,000 step-long energy minimization with steep descent algorithm. Thereafter, the solution of the system was equilibrated by 400 ps constant volume simulation at the temperature of 30 K, 200 ps constant pressure simulation at 300 K, and finally, 200-ps constant volume simulation at 300 K. Minimized and equilibrated system of each model was used for 50 ns molecular dynamics simulation with a system temperature of 300 K.

2.14. Native ion mobility-mass spectrometry

Prior to native IMMS experiments, protein samples were buffer exchanged into 200 mM ammonium acetate solution (pH 7.4) using centrifugal gel filtration columns MicroBio-Spin P-6 by Bio-Rad (Hercules, CA, USA). The samples diluted to 10 μM concentration were then introduced into a Synapt G2Si quadrupole-time-of-flight mass spectrometer from Waters (Milford, MA, USA) by nanoelectrospray ionization from in-house-prepared gold-coated glass capillaries [47]. The instrument conditions were carefully optimized to minimize ion activation in the gas phase while providing good ion mobility separation. Namely, capillary, sampling cone, trap collisional energy, and trap DC bias voltages were set to 1.0 kV, 10 V, 2 V, and 22 V, respectively. Source temperature was kept at 20 °C, whereas gas flows were 6 ml/min for argon in the trap collision cell, 180 ml/min for helium cooling window, and 60 ml/min for nitrogen in the mobility cell. Travelling potential wave in the ion mobility cell had 25 V fixed height, whereas its velocity was systematically varied between 250 and 850 m/s in 100 m/s increments.

External mass calibration was performed using a 25-mg/ml cesium iodide solution. Ion mobility arrival time distributions were extracted using MassLynx 4.1 software by Waters (Milford, MA, USA) and were used to estimate the collisional cross sections in helium (^{He}CCS) for the sample ions following a procedure described previously [48]. For this purpose, ion mobility was calibrated by ions of known ^{He}CCS [49,50], namely bovine ubiquitin, equine cytochrome *c*, and bovine beta-lactoglobulin (monomeric and dimeric forms), which were analyzed under conditions identical to those of Nkrp1b samples. Finally, for comparison with experimental results, theoretical ^{He}CCS values were calculated for modeled Nkrp1b structures by the projection approximation method implemented in the IMPACT program [51] and were scaled, as described previously, to compensate for scattering and long-range interactions underestimated by projection approximation [52,53].

3. Results and discussion

3.1. Nkrp1b protein sequence alignment

Crystallography-based structural models of two Nkrp1 family members (activating Nkrp1a and inhibitory Nkrp1b, both from C57BL/6 mouse strain) are available [27–30], but Nkrp1b from other mouse strains have not yet been studied. As we intended to derive a representative Nkrp1b structure and describe the behavior of this protein under native conditions, it was first necessary to select the most suitable template for initial molecular modeling. Therefore, multiple protein sequence alignment was performed to choose an Nkrp1b sequence from the most representative mouse strain (BALB/c, 129S6, or SJL/J) and an appropriate modeling template (crystal structure of Nkrp1b or Nkrp1a from C57BL/6 mouse strain).

The Nkrp1b CTLDs of the first three mentioned laboratory mice strains (BALB/c, 129S6, or SJL/J) are mutually highly homologous (≥98% identity). However, Nkrp1b (C57BL/6) shares only 85% sequence identity with Nkrp1b from the other strains. Even more importantly, Nkrp1b (C57BL/6) also contains two additional cysteines and a threonine instead of proline at position 161 (highlighted in red in

```
Nkrp1b(BALB/c)      SVNLECPQDWLSHRDKCFRVFQVSNTWEEGQADCGRKGATLLLIQDQEELRFLLDSIKEK
Nkrp1b(129S6)       SVNLECPQDWLSHRDKCFRVFQVSNTWEEGQADCGRKGATLLLIQDQEELRFLLDSIKEK
Nkrp1b(SJL/J)       SVNLECPQDWLSHRDKCFRVFQVSNTWEEGQADCGRKGATLLLIQDQEELRFLLDSIKEK
Nkrp1b(C57BL/6)     SAKLECPQDWLSHRDKCFHVSQVSNTWKECRIDCDKKGATLLLIQDQEELRFLLDSIKEK
Nkrp1a(C57BL/6)     SAKLECPQDWLSHRDKCFHVSQVSNTWEEGLVDCDGKGATLMLIQDQEELRFLLDSIKEK
                    *.:***************:* ******:*   **. *****:******************

Nkrp1b(BALB/c)      YNSFWIGLRFTLPDMNWKWINGTTFNSDVLKITGVTENGSCATISGDKVTSESCSTDNRW
Nkrp1b(129S6)       YNSFWIGLRFTLPDMNWKWINGTTFNSDVLKITGVTENGSCATISGDKVTSESCSTDNRW
Nkrp1b(SJL/J)       YNSFWIGLRFTLPDMNWKWINGTTFNSDVLKITGDTENGSCASISGDKVTSESCSTDNRW
Nkrp1b(C57BL/6)     YNSFWIGLSYTLTDMNWKWINGTAFNSDVLKITGVTENGSCAAISGEKVTSEGCSSDNRW
Nkrp1a(C57BL/6)     YNSFWIGLRYTLPDMNWKWINGSTLNSDVLKITGDTENDSCAAISGDKVTFESCNSDNRW
                    ******** :** *********:::********* ***.***:***:*** *.*.:****

Nkrp1b(BALB/c)      ICQKELNHKTPSNDS----
Nkrp1b(129S6)       ICQKELNHKTPSNDS----
Nkrp1b(SJL/J)       ICQKELNHETPSND-----
Nkrp1b(C57BL/6)     ICQKELNHETPCNDS----
Nkrp1a(C57BL/6)     ICQKELYHETLSNYVGYGH
                    ****** *:* .*
```

Fig. 1. Sequence alignment of CTLDs of different Nkrp1b receptors and an Nkrp1a receptor. Nkrp1b proteins from the mouse strains BALB/c, 129S6, and SJL/J are highly homologous (≥98% identity), but they share only 85% sequence identity with Nkrp1b (C57BL/6). Nkrp1a (C57BL/6), which we used as a template for Nkrp1b homology modeling, also shares 84% sequence identity with Nkrp1b (BALB/c) but lacks additional cysteines and Pro- > Thr mutation present in the sequence of Nkrp1b (C57BL/6), as highlighted in red. Asterisk (*) indicates conserved residues, colon marks (:) indicate amino acids of highly similar properties, period (.) indicates amino acids of weakly similar properties, and gap () indicates no similar properties between amino acids.

Fig. 1), which contrasts with Nkrp1b variants of all other strains. This may significantly affect the fold and function of this protein, thus making it less suited as a general representative of Nkrp1b conformation in all common mice strains.

Surprisingly, Nkrp1a also shows 84% sequence identity with Nkrp1b (BALB/c), 84% with Nkrp1b (129S6), and 86% with Nkrp1b (SJL/J). Moreover, Nkrp1a does not contain the extra cysteines and does not lack the proline. Thus, the Nkrp1b (BALB/c) structure was deemed to be likely more similar to the structure of the activating isoform Nkrp1a (C57BL/6) than to the inhibitory Nkrp1b (C57BL/6). Therefore, we endeavored to study Nkrp1b (BALB/c) in our experiments as a representative of the more sequentially conserved group.

3.2. Intact protein characterization and disulfide bond mapping

Although the Nkrp1 proteins have so far been considered to naturally occur as homodimers dimerizing through cysteines in their stalk regions, we generated the whole ectodomain (starting with Val63) and the ligand-binding domain lacking the stalk (starting with Ser89) of the Nkrp1b (BALB/c) using bacterial expression. Following a rapid dilution refolding, size-exclusion chromatography was used to purify the recombinant proteins. Besides the majority of proteins was present in aggregated state, both protein variants regardless of the presence of the stalk region were detected folded as both monomers (fractions 3) and homodimers (fractions 2) in size-exclusion chromatography/SDS-PAGE analysis (Fig. 2).

To further ascertain the identity of protein samples, the samples were analyzed using ultra-high resolution MS. The measured molecular masses were 18,353.78 Da and 15,453.41 Da for Nkrp1b with and without stalk, respectively. When compared with calculated theoretical masses of the native proteins (18,353.77 Da and 15,453.38 Da), the resulting measurement errors of 0.5 ppm and 1.9 ppm proved that all cysteines in our Nkrp1b constructs were linked by disulfide bonds.

To exactly determine the disulfide linkages in Nkrp1b with the focus on the bonds in the stalk, we used bottom-up LC-MS analyses of enzymatically digested proteins. According to the entire Nkrp1b protein sequence numbering, we identified disulfide linkages Cys94-Cys105, Cys122-Cys210, and Cys189-Cys202. This corresponds to the common pattern typical for CTLRs, as determined previously [16]. According to our experimental data, the two additional cysteines (Cys75 and Cys88) in the stalk region of Nkrp1b were connected in two different ways. In one case, both cysteines created an intermolecular disulfide bridge with the same cysteines in the second molecule (Cys75-Cys75 and Cys88-Cys88). In another case, the first two cysteines in Nkrp1b were linked together (Cys75-Cys88) within one protein molecule. All data are presented in Table S1. Therefore, this directly confirms that Nkrp1b is a mixture of monomers and homodimers in solution.

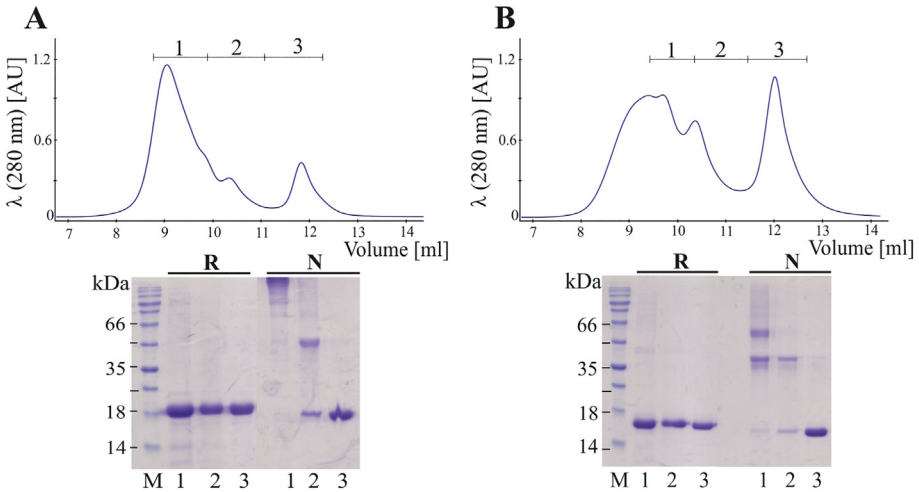

Fig. 2. Nkrp1b protein purification by size-exclusion chromatography and fraction analysis by SDS-PAGE. Results for protein variant (A) containing the stalk (molecular weight, 18.4 kDa) and (B) lacking the stalk (molecular weight, 15.5 kDa). Protein fractions 1–3 obtained by size-exclusion chromatography correspond to the numbering of lanes in the SDS-PAGE gels. Fractions were analyzed under reducing (R) and nonreducing (N) conditions; "M" symbolizes a protein marker.

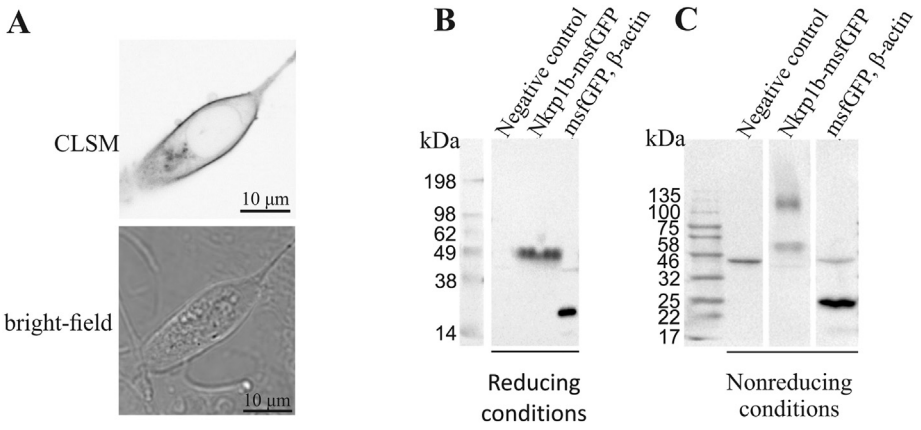

Fig. 3. Nkrp1b localization in a cell and immunoblotting analysis. (A) CLSM images of msfGFP-tagged Nkrp1b. The image from the GFP channel is shown above, matching bright-field image below. Using anti-GFP antibody, Nkrp1b-msfGFP was detected (B) as a monomer (55 kDa) under reducing conditions and (C) as a mixture of monomer and homodimer (110 kDa) under nonreducing conditions. A negative control (untransfected cells) served as a test of the specificity of the anti-GFP antibody.

3.3. Immunoblotting of Nkrp1b-msfGFP expressed in mammalian cells confirms that Nkrp1b is present as a mixture of monomers and homodimers also on a cell surface

To examine the oligomerization state of Nkrp1b *in vivo*, the full-length protein tagged with monomeric superfolder (msf) GFP was expressed in the mammalian COS-7 cell line. Initially, the localization of Nkrp1b was determined by confocal laser scanning microscopy (CLSM), which confirmed that the expressed protein is indeed present on the cell surface (Fig. 3A). Next, the protein was analyzed by western blotting with the tagged Nkrp1b detected using a polyclonal anti-GFP antibody (Fig. 3B and 3C). Under reducing conditions, only monomeric Nkrp1b-msfGFP (55 kDa) was present. However, nonreducing conditions showed the protein in both its states, monomeric and dimeric (110 kDa). Therefore, this approach further corroborates Nkrp1b to be a mixture of monomers and homodimers both recombinantly expressed and purified from bacteria and in a mammalian cell line. A negative control served as a test of the specificity of the anti-GFP antibody. Accordingly, no signal was detected for the untransfected cell line when incubated with the antibody. On the other hand, msfGFP itself, as a positive control, was found to be 27 kDa, which corresponds to its theoretical molecular weight. In addition, β-actin (43 kDa) served as a loading control.

3.4. Only monomeric forms of Nkrp1b are functionally active

To examine, which of the Nkrp1b variants are biologically active, and therefore capable of interacting with the ligand, all our protein variants were labeled with ATTO 590 fluorescent dye and incubated with bone marrow-derived cells expressing an Nkrp1b ligand on their surface [12]. The lectin PNA from *Arachis hypogaea* (peanut), which was used as a positive control, belongs to the same protein superfamily as Nkrp1b and specifically binds to D-galactosyl residues of glycosylated membrane proteins [54]. The method of scanning fluorescence microscopy was then used to assess, which labeled Nkrp1b protein variants interacted with the cells.

Using this method, it was revealed that only monomeric Nkrp1b forms could bind to the cells, irrespective of the presence of the stalk region, as shown by the representative microscope images (Fig. 4A). The plot in Fig. 4B shows the dependence of the mean intensity of the red (ATTO 590 or Alexa Fluor® 568) signal on the protein concentration (Nkrp1b or PNA). The standard errors of the mean values were below 0.3 MFI for all the points due to the large numbers of individual cell data in each data set and are therefore not visible in the plot. Red signal intensity of monomeric Nkrp1b forms and of positive control increased with increasing protein concentration, whereas that of dimeric Nkrp1b forms did not change with their increasing concentration. This clearly indicates that our dimeric Nkrp1b variants do not interact with cells.

Our results correspond to the known interaction mode of Nkrp1b:m12 and NKp65:KACL as both the proteins (Nkrp1b from C57BL/6 mice and human NKp65) interact as monomers. A recent crystal structure of Nkrp1b interacting with m12 *via* a polar claw mechanism shows that two Nkrp1b molecules clench the dimer of m12 and do not contact each other. On the contrary, two monomers of NKp65 (a human homologue of Nkrp1b) symmetrically engage a dimeric KACL (a homologue of Clr proteins) in a bivalent binding mode. It means that two NKp65 molecules identically contact KACL binding sites and the authors concluded that in fact, NKp65 dimerize after ligand binding [30,55]. Based on these findings and in the context with our microscopy data, two Nkrp1b molecules may separately participate in the interaction or the interaction may promote induced Nkrp1b dimerization. In addition, interaction process can be dependent on a specific ligand as such behavior has previously been demonstrated for the Ly49H receptor, which binds MHC class I molecules or the immunoevasin m157 [56]. Nevertheless, it seems that Nkrp1b enters the interaction as monomer in either cases.

3.5. Chemical cross-linking and homology modeling of Nkrp1b

To obtain structural models of Nkrp1b, homology modeling in combination with experimentally obtained distance restraints (from intra- and intermolecular chemical cross-linking and disulfide bond mapping) was used.

3.5.1. Intramolecular chemical cross-linking

Intramolecular cross-linking of Nkrp1b monomeric forms with DSG and DSS was performed mainly to determine the conformations of the loop and stalk regions in solution because the two high-resolution structural models of Nkrp1a (C57BL/6) differ by the loop position. The loop is either attached to a compact protein core (pdb:2MTI) or extended and participates in domain-swapping dimerization (pdb:3M9Z) similar to mannose macrophage receptor [20] or snake venom bitiscetin [21] from the same protein superfamily.

Cross-links connecting 9 out of 10 primary amines present in the CTLD were found within a monomeric Nkrp1b (BALB/c) molecule. These included Lys179 in the loop region, which was connected to Lys196 in the protein core (full results are listed in Table S2). This implies that the loop is attached to the protein core in solution, as the distance between the loop in its extended position and the CTLD would otherwise exceed the arm range of the cross-linker.

Regarding the stalk region, the N-terminus of Nkrp1b was found to be very reactive as it cross-linked with different amines in the protein domain, suggesting that at least while isolated in solution, the stalk moves rather freely around the core domain.

3.5.2. Intermolecular chemical cross-linking

Intermolecular chemical cross-linking of Nkrp1b dimeric forms was performed with a mixture of light- and heavy-isotope-labeled proteins

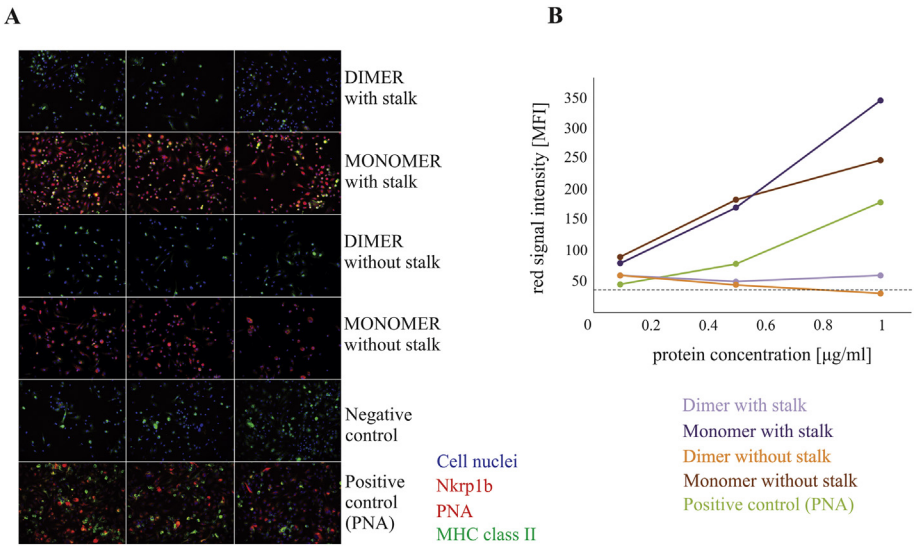

Fig. 4. Interactions of fluorescently labeled Nkrp1b protein variants with bone marrow-derived cells analyzed by scanning fluorescent microscopy. (A) Microscope images of individual Nkrp1b protein forms of 1 µg/ml concentration with cells (three representative fields of view for each sample). Cell nuclei are stained blue with DAPI, Nkrp1b or PNA (positive control) red with ATTO 590 or Alexa Fluor® 568 and MHC class II molecules green with GFP. (B) Quantitative image analysis of the red signal intensity in the microscope images. Several hundreds of cells in 36 fields of view for each sample prepared in duplicates were used for analysis. Three different concentrations (0.1 µg/ml; 0.5 µg/ml and 1 µg/ml) of labeled proteins were tested, a dashed line indicates fluorescence level of the negative control.

to determine the dimerization interface of Nkrp1b. Only cross-links detected between peptide containing ^{14}N and peptide containing ^{15}N were evaluated as the interchain connections. The cross-linking agent DSG alone was utilized in this case as it is the shortest available cross-linker, therefore, the possibility of artifacts forming was minimized.

Six unique connections were identified between the light- and heavy-isotope-labeled molecules in the dimeric Nkrp1b protein variant containing the stalk, whereas three cross-links were found in the form lacking the stalk (Table S3). No cross-links were found between N-termini or primary amines present in the stalk region, which is also consistent with results of intramolecular chemical cross-linking, where the stalk region was shown to move around the CTLD and interact with lysines in the protein core. These results indicate that the dimerization interface is located between CTLDs, but not in the stalk region, as visualized in Fig. 5A.

Together, the intermolecular chemical cross-linking along with the disulfide bond mapping proved that the stalk does not play a key role in protein dimerization. Moreover, fluorescence microscopy experiments described above demonstrated that the stalk is not even necessary for Nkrp1b to be functionally active for binding to its ligand.

3.5.3. Homology modeling and molecular dynamics simulations

To obtain a complete structural model of Nkrp1b (BALB/c), we combined our experimental constraints derived by the above-described structural MS methods with molecular modeling. An NMR structure (pdb:2MTI) and two crystal structures (pdb:3M9Z, 3T3A) of Nkrp1a (C57BL/6) were used as modeling templates (Fig.S1) as this protein shares 84% sequence identity with our studied protein Nkrp1b (BALB/c) and does not possess the additional disulfide bridge that Nkrp1b (C57BL/6) carries. In addition, distinct existing structural models of Nkrp1a (differing by the loop position) allowed us to build on multiple possible protein conformations and to choose the homology model that best corresponded to our experimental data.

Moreover, structural modeling and molecular dynamics were performed to determine the possible conformation of the Nkrp1b stalk region in solution, as no template for modeling this region of the protein is available yet. An *ab initio* modeling of the stalk region (residues Val63-Asp87) suggested that the presence of an α-helix at residues SSVQKICADVQEN is likely (data not shown). This could also be related to the structure of the carbohydrate recognition and stalk domains of surfactant protein A (pdb:1R13). However, the presence of this helix could not be reconciled with the experimental collision cross section (CCS) constraints derived by native IMMS measurements (described in the following section). With the helix in place, the CCS of our models was significantly higher than our experimental values. Therefore, we believe that at least in the case of our recombinantly expressed soluble protein forms, when Nkrp1b is not attached to any membrane, its stalk is rather unstructured and flexible.

Indeed, such a behavior was also observed in the modeling results, when 10 homology models of each Nkrp1b protein variant were selected based on minimal energy (dispersion of CCS values among these models is shown in Table S4) and mutually aligned to compare differences between their structures (Fig.S2A). The alignment showed the CTLDs, including the loop regions and short unstructured C-termini to be rather well defined. However, very different stalk positions were discovered in individual Nkrp1b models, as no useful template is available for this protein region. This fits nicely with our complementary data from both native IMMS and cross-linking experiments.

Finally, full molecular dynamics simulations (50 ns) of the selected Nkrp1b protein variants were performed to examine the stability of the proteins and movements of their stalks in solution (Fig. S2B). Analyses of the modeling trajectories by monitoring the root-mean-square deviation (RMSD) showed that the CTLDs remained stable in all studied protein variants. Only N-terminal part of the monomeric Nkrp1b form without stalk slightly moved on this timescale. Moreover, the stalk regions of both chains of dimeric Nkrp1b exhibited rather unhindered movement in solution, with occasional weak non-covalent interactions with other protein residues. The RMSD analyses proved and chemical cross-linking confirmed that the stalk can move freely around the CTLD.

Taken together, our data allowed us to build the complete model of the Nkrp1b protein, with and without the stalk, including their dimeric forms, as shown in Fig. 5.

3.6. Native ion mobility-mass spectrometry and correlation with the results of homology modeling

To validate our structural models, CCS of all four Nkrp1b protein variants were measured under very gentle electrospray and MS instrument conditions to compare them with theoretical values of computed homology models and to select the most appropriate Nkrp1b structures, as described previously [57].

The spectra of Nkrp1b protein variants (Fig. 6) showed the ratio of monomeric/dimeric Nkrp1b forms in the observed charge states of measured samples and proteins. The mixture of monomers and homodimers was observed in all samples (except for the monomer without the stalk) because it was not possible to separate the forms completely during purification, as revealed also by gel electrophoresis. Also, it is important to point out that dimers formation is rather dynamic thus

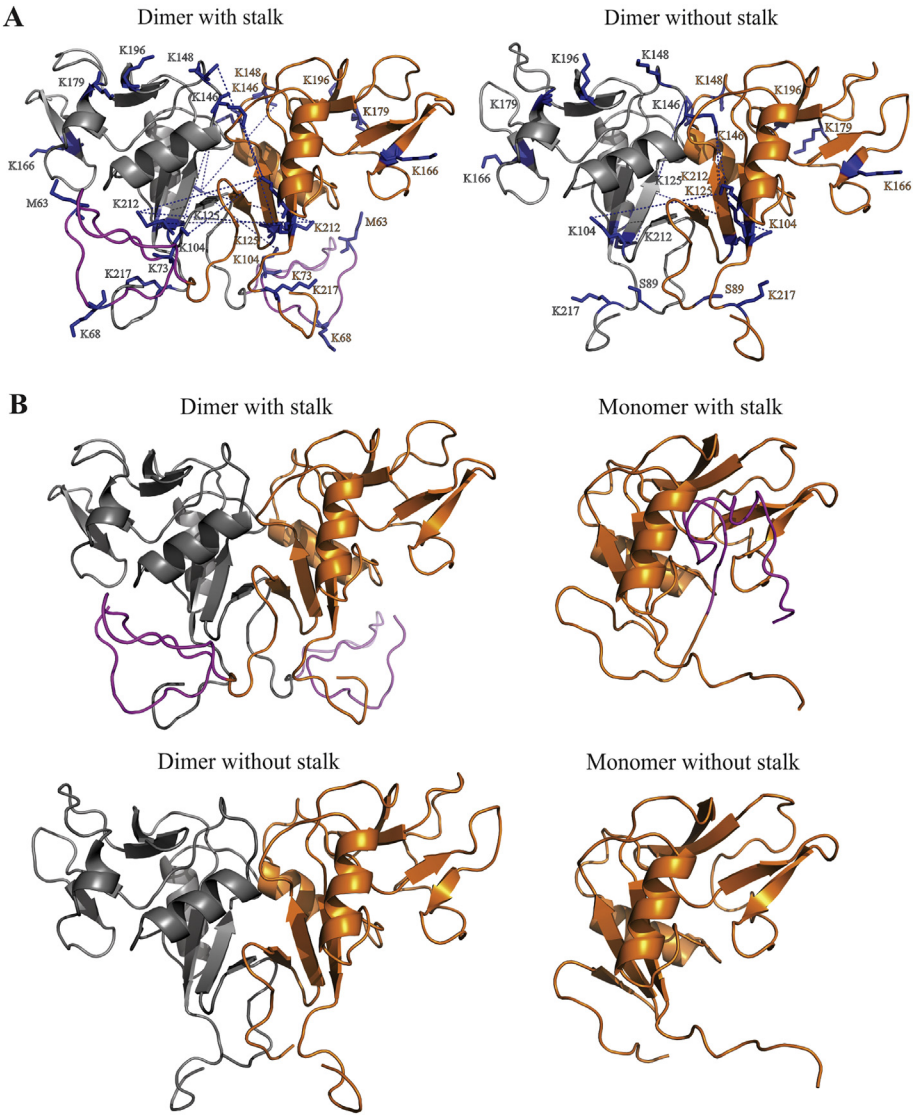

Fig. 5. Visualization of intermolecular cross-links and structure of Nkrp1b protein variants. (A) Visualization of Nkrp1b dimerization interface using intermolecular cross-links (blue dotted lines). Primary amines are displayed as blue side chains; sequence numbering corresponds to the whole Nkrp1b protein. First amino acids in the Nkrp1b protein variants are Met63 or Ser89. (B) Homology models of dimeric/monomeric Nkrp1b protein forms containing/lacking the stalk region (highlighted in magenta), whose parameters best correlate with experimental data.

there is monomer/dimer equilibrium in solution.

A comparison of CCSs of computed Nkrp1b models and values measured by IMMS is shown in Table 1. As we observed no significant systematic differences between various ion mobility settings (with a small caveat discussed below), CCSs averaged across all travelling wave velocities, and charge states are reported with their interval of total estimated analysis error (E_{tot}). This error value combines a standard deviation obtained from the CCS values used for averaging, an experimental calibration fit error, and an inherent uncertainty (~1%) associated with the CCS values of standard proteins used for calibration [58]. The theoretical and experimental data generally correlate very well, with some slight deviation for dimeric Nkrp1b with stalk and monomeric Nkrp1b without stalk, wherein experimental CCS values are slightly lower than the computed ones. CCSs of all used theoretical models as well as values for different charge states of the measured proteins and all travelling wave velocities are listed in Table S5.

Observed CCSs of monomers were very consistent across all travelling wave velocities (all data are shown in Table S5), which proves that the instrument parameters were gentle enough to retain a folded protein structure during our measurements irrespective of the time the ions spent in a mobility cell. However, CCS of both dimeric forms (and especially of the one with the stalk) increased slightly with increased wave speed (and longer time spent in the mobility cell). In addition, CCSs of both dimeric forms did not vary between particular charge states. As we know that the structure of individual monomers is stable on this time scale, we hypothesize that this phenomenon can be attributed to some degree of remaining quaternary structure flexibility when the Nkrp1b molecules would slightly move within the dimer relative to each other.

Regarding different charge states, a Coulombic unfolding was negligible apart from the highest (9+) charge state of Nkrp1b monomer with stalk. CCS values for this protein variant of charge states 7+ and 8+ across all travelling wave velocities are consistent with standard deviation < 7. Values for 9+ charge state are > 100 $Å^2$ higher and standard deviation was 19. This implies that higher charge state causes partial Coulombic unfolding of protein in this case. Therefore, 9+ charge state of Nkrp1b monomer with stalk was excluded from calculations. Considering CCS values for monomer without stalk of charge states 6+, 7+ and 8+, the difference between the lowest and highest charge state is < 60 $Å^2$ and standard deviation for 8+ charge state is 9.

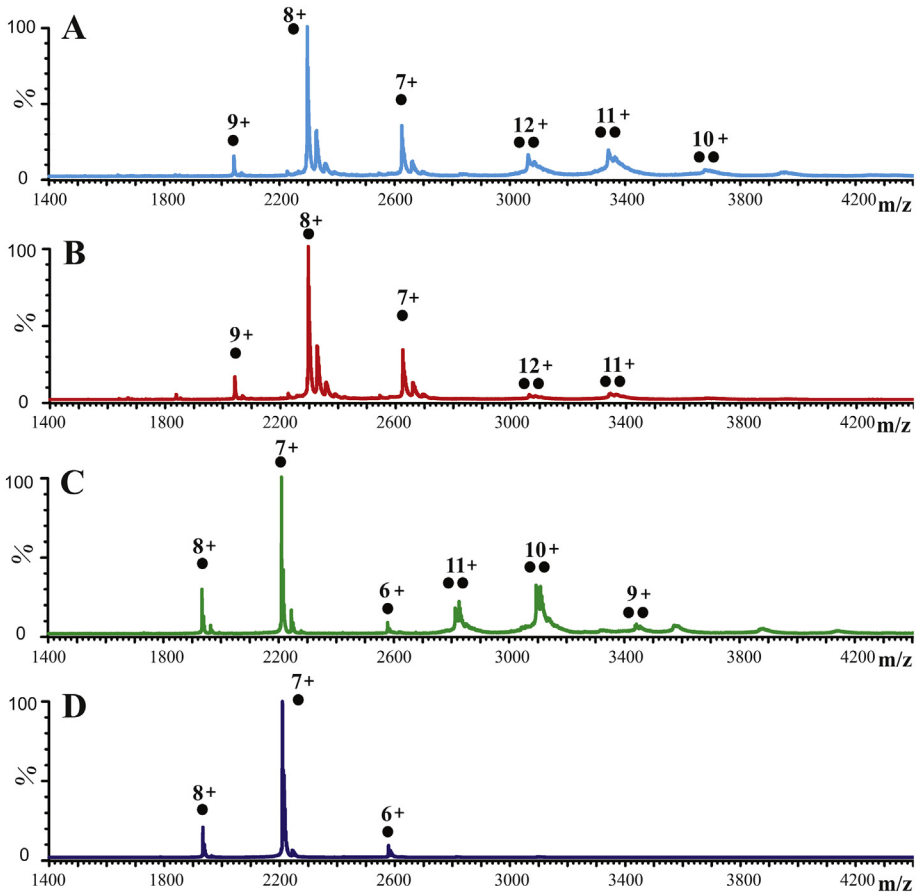

Fig. 6. Representative native mass spectra of Nkrp1b protein variants as used for ion mobility analyses. (A) Dimer with stalk, (B) monomer with stalk, (C) dimer without stalk, and (D) monomer without stalk. Charge states and monomeric/dimeric conformations (shown as dots) of Nkrp1b protein variants are marked. The presence of monomeric and dimeric protein variants in individual spectra may be associated with partial complex dissociation in ammonium acetate and incomplete separation by the size-exclusion chromatography.

Table 1
Experimental and modeled CCSs of Nkrp1b protein forms. The average CCS values of theoretical homology models and values determined by native IMMS experiments. Total estimated error (E_{tot}) of measurements is included.

Protein form	Homology models CCS [Å^2]	Experimental CCS ± E_{tot} [Å^2]
Dimer with stalk	2781	2625 ± 102
Monomer with stalk	1591	1629 ± 34
Dimer without stalk	2336	2311 ± 74
Monomer without stalk	1535	1469 ± 36

Therefore, this charge state was deemed to be still consistent with lower charge states of monomer without stalk.

Experimental CCS values of Nkrp1b proteins were compared with calculated variants of several homology models. CCS of a monomeric Nkrp1b homology model (without stalk) with the loop in an extended position was 1829 Å^2. Our experimentally derived CCS of the native-like protein was 1469 ± 36 Å^2 (Table 1), which corresponds better to 1535 Å^2 in the homology model with the loop attached to the protein core. Similarly, CCS of dimeric Nkrp1b homology model (without stalk) with the extended loops was 2662 Å^2. CCS of our selected Nkrp1b dimeric model (without stalk) was 2336 Å^2, which correlates better to the experimental value of 2311 ± 74 Å^2 (Table 1). Overall, these results fit in nicely with our data from chemical cross-linking in terms of both loop orientation and stalk region flexibility.

4. Conclusions

Although CTLRs are generally structurally conserved, their protein sequences and functions are divergent as they bind saccharides in complex with Ca^{2+} ions or various proteins [16]. Protein ligands of CTLRs are derived from a host cell or a virus, and their interactions differ according to their origin [30,56]. Furthermore, receptors bind their protein ligands in a promiscuous manner, and conversely, one particular ligand often targets several different CTLRs [11,25,59]. As the specific nature of these interactions is based on the structure and functional properties of a receptor, determination of the structure greatly contributes to our understanding of a receptor's function and regulation of cellular responses. In this work, we studied the effect of specific structural characteristics of the inhibitory receptor Nkrp1b on its conformation and molecular interactions.

Certain structural features, which can highly influence the conformation and interactions of Nkrp1b, involve its long loop region, flexible stalk, and its oligomerization state. Two Nkrp1b protein variants were recombinantly prepared to investigate the function of the stalk: the whole ectodomain and the ligand-binding domain lacking the stalk. It was observed that both variants fold as monomers and homodimers *in vitro*. Similar behavior was achieved *in vivo* as well, where the analysis of cell lysates of mammalian cells revealed Nkrp1b as a mixture of monomers and homodimers. MS analysis of recombinant proteins revealed that the Nkrp1b forms monomers and covalent or non-covalent dimers. According to disulfide bond mapping, two cysteines in the stalk may be intermolecularly linked by two covalent bonds or the cysteines within one molecule can be connected.

Furthermore, the biological activity of all these Nkrp1b forms was tested. It was observed that only monomeric Nkrp1b forms could interact with their ligands on a cell surface, whereas homodimers were not functional. Moreover, the presence of the stalk did not influence the interaction, and it was not even crucial for protein dimerization. Finally, based on experimental data provided by a range of structural MS techniques and homology modeling, Nkrp1b ectodomain structural models in its monomeric and dimeric conformations were proposed.

In conclusion, we demonstrated that the stalk does not affect the

fold of CTLD or the ability of Nkrp1b to interact with its ligands and that the stalk is not necessary for the receptor dimerization as was considered for decades. In addition, our data clearly demonstrated that the loop region is attached to the compact core of the receptor and that it does not participate in domain swapping in contrast to the activating Nkrp1a receptor. Finally, the fact that Nkrp1b can form dimers, which are not functional, opens the possibility of their regulatory function, which could be the topic of interest for future research.

Supplementary data to this article can be found online at https://doi.org/10.1016/j.jprot.2018.11.007.

Author contributions

P. Novák planned the mass spectrometric experiments and supervised the manuscript writing. L. Hernychová performed protein sequence alignment, protein production including isotopically labeled protein variants, prepared samples for MS measurements and analyzed acquired data (including IMMS), labeled Nkrp1b protein variants with fluorescence dye, created pictures and wrote the manuscript. M. Rosůlek carried out MS measurements. A. Kádek performed IMMS measurements. L. Adámková cloned msfGFP-tagged Nkrp1b and characterized its cellular localization and oligomerization on mammalian cell surface. V. Grobárová cultivated bone marrow cells and supervised subsequent interactions of Nkrp1b. O. Šebesta performed scanning fluorescence microscopy. Z. Kukačka designed chemical cross-linking. K. Skála participated in recombinant protein production. V. Spiwok and J. Chmelík supervised the homology modeling and molecular dynamics simulations, which were performed by V. Mareška. J. Černý designed bone marrow cells cultivation and their interaction with labeled protein variants of Nkrp1b.

Acknowledgement

This work was supported by the Charles University Grant Agency, Czech Republic (200816), the Czech Science Foundation, Czech Republic (grant numbers 16-24309S), the Ministry of Education of the Czech Republic, Czech Republic (projects LH15010, LD15089; program “NPU II” projectLQ1604; LM2015043 CIISB for CMS BIOCEV; LTC17065), COST Action (BM1403), European Regional Development Funds (CZ.1.05/1.1.00/02.0109 BIOCEV), European Commission H2020 (European Network of Fourier-Transform Ion-Cyclotron-Resonance Mass Spectrometry Centers - project agreement No.731077) and, in part, by the Czech Academy of Sciences, Czech Republic (RVO61388971).

Microscopy was performed in the Laboratory of Confocal and Fluorescence Microscopy co-financed by the European Regional Development Fund and the State Budget of the Czech Republic. Project no. CZ.1.05/4.1.00/16.0347 and CZ.2.16/3.1.00/21515. We acknowledge the Imaging Methods Core Facility at BIOCEV, an institution supported by the Czech-BioImaging large RI projects (LM2015062 and CZ.02.1.01/0.0/0.0/16_013/0001775, funded by MEYS CR), for their support with image data analysis presented in this paper.

Declaration of interest

The authors declare that they have no conflicts of interests relating to the contents of this article.

References

[1] E. Vivier, E. Tomasello, M. Baratin, T. Walzer, S. Ugolini, Functions of natural killer cells, Nat. Immunol. 9 (2008) 503–510, https://doi.org/10.1038/ni1582.
[2] J. Villard, The role of natural killer cells in human solid organ and tissue transplantation, J. Innate Immun. 3 (2011) 395–402, https://doi.org/10.1159/000324400.
[3] Z. Tian, M.E. Gershwin, C. Zhang, Regulatory NK cells in autoimmune disease, J. Autoimmun. 39 (2012) 206–215, https://doi.org/10.1016/j.jaut.2012.05.006.
[4] C.B. Mathias, L.A. Guernsey, D. Zammit, C. Brammer, C.A. Wu, R.S. Thrall, H.L. Aguila, Pro-inflammatory Role of Natural Killer cells in the development of Allergic Airway Disease Clin. Exp. Allergy J. Br. Soc. Allergy Clin. Immunol. (2014). doi:10.1111/cea.12271
[5] E.E. Winger, J.L. Reed, The multiple faces of the decidual natural killer cell, Am. J. Reprod. Immunol. 70 (2013) 1–9, https://doi.org/10.1111/aji.12103.
[6] K.S. Campbell, A.K. Purdy, Structure/function of human killer cell immunoglobulin-like receptors: lessons from polymorphisms, evolution, crystal structures and mutations, Immunology. 132 (2011) 315–325, https://doi.org/10.1111/j.1365-2567.2010.03398.x.
[7] O.A. Aguilar, A. Mesci, J. Ma, P. Chen, C.L. Kirkham, J. Hundrieser, S. Voigt, D.S.J. Allan, J.R. Carlyle, Modulation of Clr ligand expression and NKR-P1 receptor function during murine cytomegalovirus infection, J. Innate Immun. (2015), https://doi.org/10.1159/000382032.
[8] K. Kärre, H.G. Ljunggren, G. Piontek, R. Kiessling, Selective rejection of H-2-deficient lymphoma variants suggests alternative immune defence strategy, Nature. 319 (1986) 675–678, https://doi.org/10.1038/319675a0.
[9] J.R. Carlyle, A.M. Jamieson, S. Gasser, C.S. Clingan, H. Arase, D.H. Raulet, Missing self-recognition of Ocil/Clr-b by inhibitory NKR-P1 natural killer cell receptors, Proc. Natl. Acad. Sci. U. S. A. 101 (2004) 3527–3532, https://doi.org/10.1073/pnas.0308304101.
[10] S.K. Kung, R.C. Su, J. Shannon, R.G. Miller, The NKR-P1B gene product is an inhibitory receptor on SJL/J NK cells, J. Immunol. 162 (1999) 5876–5887 http://www.ncbi.nlm.nih.gov/pubmed/10229823 (accessed May 11, 2015).
[11] P. Chen, S. Bélanger, Q. Aguilar, A. Zhang, M.M.A. St-Laurent, A.P. Rahim, J.R. Carlyle Makrigiannis, Analysis of the mouse 129-strain Nkrp1-Clr gene cluster reveals conservation of genomic organization and functional receptor-ligand interactions despite significant allelic polymorphism, Immunogenetics. 63 (2011) 627–640, https://doi.org/10.1007/s00251-011-0542-8.
[12] Q. Zhang, M.M. a Rahim, D.S.J. Allan, M.M. Tu, S. Belanger, E. Abou-Samra, J. Ma, H.S. Sekhon, T. Fairhead, H.S. Zein, J.R. Carlyle, S.K. Anderson, A.P. Makrigiannis, Mouse Nkrp1-Clr gene cluster sequence and expression analyses reveal conservation of tissue-specific MHC-independent immunosurveillance, PLoS One. 7 (2012) e50561, https://doi.org/10.1371/journal.pone.0050561.
[13] S. Voigt, A. Mesci, J. Ettinger, J.H. Fine, P. Chen, W. Chou, J.R. Carlyle, Cytomegalovirus evasion of innate immunity by subversion of the NKR-P1B:Clr-b missing-self axis, Immunity. 26 (2007) 617–627, https://doi.org/10.1016/j.immuni.2007.03.013.
[14] K.J.N. Williams, E. Wilson, C.L. Davidson, O.A. Aguilar, L. Fu, J.R. Carlyle, D.N. Burshtyn, Poxvirus infection-associated downregulation of C-type lectin-related-b prevents NK cell inhibition by NK receptor protein-1B, J. Immunol. 188 (2012) 4980–4991, https://doi.org/10.4049/jimmunol.1103425.
[15] J.H. Fine, P. Chen, A. Mesci, D.S.J. Allan, S. Gasser, D.H. Raulet, J.R. Carlyle, Chemotherapy-induced genotoxic stress promotes sensitivity to natural killer cell cytotoxicity by enabling missing-self recognition, Cancer Res. 70 (2010) 7102–7113, https://doi.org/10.1158/0008-5472.CAN-10-1316.
[16] A.N. Zelensky, J.E. Gready, The C-type lectin-like domain superfamily, FEBS J. 272 (2005) 6179–6217, https://doi.org/10.1111/j.1742-4658.2005.05031.x.
[17] K. Drickamer, C-type lectin-like domains, Curr. Opin. Struct. Biol. 9 (1999) 585–590 http://www.ncbi.nlm.nih.gov/pubmed/10508765 accessed June 3, 2016.
[18] A.N. Zelensky, J.E. Gready, Comparative analysis of structural properties of the C-type-lectin-like domain (CTLD), Proteins. 52 (2003) 466–477, https://doi.org/10.1002/prot.10626.
[19] Z. Sovová, V. Kopecký, T. Pazderka, K. Hofbauerová, D. Rozbeský, O. Vaněk, K. Bezouška, R. Ettrich, Structural analysis of natural killer cell receptor protein 1 (NKR−P1) extracellular domains suggests a conserved long loop region involved in ligand specificity, J. Mol. Model. 17 (2011) 1353–1370, https://doi.org/10.1007/s00894-010-0837-y.
[20] H. Feinberg, S. Park-Snyder, A.R. Kolatkar, C.T. Heise, M.E. Taylor, W.I. Weis, Structure of a C-type carbohydrate recognition domain from the macrophage mannose receptor, J. Biol. Chem. 275 (2000) 21539–21548, https://doi.org/10.1074/jbc.M002366200.
[21] S. Hirotsu, H. Mizuno, K. Fukuda, M.C. Qi, T. Matsui, J. Hamako, T. Morita, K. Titani, Crystal structure of bitiscetin, a von Willebrand factor-dependent platelet aggregation inducer, Biochemistry. 40 (2001) 13592–13597 http://www.ncbi.nlm.nih.gov/pubmed/11695907 accessed June 3, 2016.
[22] P. Li, D.L. Morris, B.E. Willcox, A. Steinle, T. Spies, R.K. Strong, Complex structure of the activating immunoreceptor NKG2D and its MHC class I-like ligand MICA, Nat. Immunol. 2 (2001) 443–451, https://doi.org/10.1038/87757.
[23] W.H. Chambers, N.L. Vujanovic, A.B. DeLeo, M.W. Olszowy, R.B. Herberman, J.C. Hiserodt, Monoclonal antibody to a triggering structure expressed on rat natural killer cells and adherent lymphokine-activated killer cells, J. Exp. Med. 169 (1989) 1373–1389 http://www.pubmedcentral.nih.gov/articlerender.fcgi?artid=2189246&tool=pmcentrez&rendertype=abstract (accessed November 4, 2014).
[24] L.L. Lanier, C. Chang, J.H. Phillips, Human NKR−P1A. A disulfide-linked homodimer of the C-type lectin superfamily expressed by a subset of NK and T lymphocytes, J. Immunol. 153 (1994) 2417–2428 http://www.ncbi.nlm.nih.gov/pubmed/8077657 (accessed November 6, 2014).
[25] K. Iizuka, O.V. Naidenko, B.F.M. Plougastel, D.H. Fremont, W.M. Yokoyama, Genetically linked C-type lectin-related ligands for the NKRP1 family of natural killer cell receptors, Nat. Immunol. 4 (2003) 801–807, https://doi.org/10.1038/ni954.
[26] J. Back, E.L. Malchiodi, S. Cho, L. Scarpellino, P. Schneider, M.C. Kerzic, R.A. Mariuzza, W. Held, Distinct conformations of Ly49 natural killer cell receptors mediate MHC class I recognition in trans and cis, Immunity. 31 (2009) 598–608, https://doi.org/10.1016/j.immuni.2009.07.007.

[27] P. Kolenko, D. Rozbeský, O. Vaněk, V. Kopecký, K. Hofbauerová, P. Novák, P. Pompach, J. Hašek, T. Skálová, K. Bezouška, J. Dohnálek, Molecular architecture of mouse activating NKR-P1 receptors, J. Struct. Biol. 175 (2011) 434–441, https://doi.org/10.1016/j.jsb.2011.05.001.
[28] D. Rozbeský, D. Adámek, E. Pospíšilová, P. Novák, J. Chmelík, Solution structure of the lymphocyte receptor Nkrp1a reveals a distinct conformation of the long loop region as compared to in the crystal structure, Proteins. 84 (2016) 1304–1311, https://doi.org/10.1002/prot.25078.
[29] D. Rozbesky, P. Man, D. Kavan, J. Chmelik, J. Cerny, K. Bezouska, P. Novak, Chemical cross-linking and H/D exchange for fast refinement of protein crystal structure, Anal. Chem. 84 (2012) 867–870 10.1021/ac202818m.
[30] O.A. Aguilar, R. Berry, M.M.A. Rahim, J.J. Reichel, B. Popović, M. Tanaka, Z. Fu, G.R. Balaji, T.N.H. Lau, M. Tu, C.L. Kirkham, A.B. Mahmoud, A. Mesci, A. Krmpotić, D.S.J. Allan, A.P. Makrigiannis, S. Jonjić, J. Rossjohn, J.R. Carlyle, A. Viral Immunoevasin, Controls Innate Immunity by Targeting the Prototypical Natural Killer Cell Receptor Family, Cell. 169 (2017) 58–71, https://doi.org/10.1016/j.cell.2017.03.002.
[31] F. Sievers, A. Wilm, D. Dineen, T.J. Gibson, K. Karplus, W. Li, R. Lopez, H. McWilliam, M. Remmert, J. Söding, J.D. Thompson, D.G. Higgins, Fast, scalable generation of high-quality protein multiple sequence alignments using Clustal Omega, Mol. Syst. Biol. 7 (2011), https://doi.org/10.1038/msb.2011.75.
[32] L. Hernychová, H. Mrázek, L. Ivanova, Z. Kukačka, J. Chmelík, P. Novák, Recombinant expression, *in vitro* refolding and characterizing disulfide bonds of a mouse inhibitory C-type lectin-like receptor Nkrp1b, Physiol. Res. 64 (Suppl. 1) (2015) S85–S93 http://www.ncbi.nlm.nih.gov/pubmed/26447598 (accessed October 12, 2015).
[33] P. Pompach, P. Man, D. Kavan, K. Hofbauerová, V. Kumar, K. Bezouska, V. Havlícek, P. Novák, Modified electrophoretic and digestion conditions allow a simplified mass spectrometric evaluation of disulfide bonds, J. Mass Spectrom. 44 (2009) 1571–1578, https://doi.org/10.1002/jms.1609.
[34] M. Boes, J. Cerny, R. Massol, M. Op den Brouw, T. Kirchhausen, J. Chen, H.L. Ploegh, T-cell engagement of dendritic cells rapidly rearranges MHC class II transport, Nature. 418 (2002) 983–988, https://doi.org/10.1038/nature01004.
[35] H. Karasuyama, F. Melchers, Establishment of mouse cell lines which constitutively secrete large quantities of interleukin 2, 3, 4 or 5, using modified cDNA expression vectors, Eur. J. Immunol. 18 (1988) 97–104, https://doi.org/10.1002/eji.1830180115.
[36] T. Zal, A. Volkmann, B. Stockinger, Mechanisms of tolerance induction in major histocompatibility complex class II-restricted T cells specific for a blood-borne self-antigen, J. Exp. Med. 180 (1994) 2089–2099 http://www.ncbi.nlm.nih.gov/pubmed/7964486 (accessed December 16, 2016).
[37] D. Rozbeský, M. Rosůlek, Z. Kukačka, J. Chmelík, P. Man, P. Novák, Impact of Chemical Cross-Linking on Protein Structure and Function, Anal. Chem. 90 (2018) 1104–1113, https://doi.org/10.1021/acs.analchem.7b02863.
[38] A. Shevchenko, M. Wilm, O. Vorm, M. Mann, Mass spectrometric sequencing of proteins silver-stained polyacrylamide gels, Anal Chem. 68 (1996) 850–858.
[39] M.M. Young, N. Tang, J.C. Hempel, C.M. Oshiro, E.W. Taylor, I.D. Kuntz, B.W. Gibson, G. Dollinger, High throughput protein fold identification by using experimental constraints derived from intramolecular cross-links and mass spectrometry, Proc. Natl. Acad. Sci. U. S. A. 97 (2000) 5802–5806, https://doi.org/10.1073/pnas.090099097.
[40] N. Eswar, B. Webb, M.A. Marti-Renom, M.S. Madhusudhan, D. Eramian, M. Shen, U. Pieper, A. Sali, Comparative protein structure modeling Using modeller, Curr. Protoc. Bioinforma, John Wiley & Sons, Inc., Hoboken, NJ, USA, 2006, , https://doi.org/10.1002/0471250953.bi0506s15 5.6.1–5.6.30.
[41] The Rosetta Software, RosettaCommons, https://www.rosettacommons.org/software accessed May 21, 2018.
[42] Robetta: full-chain protein structure prediction server, http://robetta.bakerlab.org accessed May 7, 2018.
[43] M. Shen, A. Sali, Statistical potential for assessment and prediction of protein structures, Protein Sci. 15 (2006) 2507–2524, https://doi.org/10.1110/ps.062416606.
[44] I. Kufareva, R. Abagyan, Methods of protein structure comparison, Methods Mol. Biol. 857 (2012) 231–257, https://doi.org/10.1007/978-1-61,779-588-6_10.
[45] A. Zemla, LGA: A method for finding 3D similarities in protein structures, Nucleic Acids Res. 31 (2003) 3370–3374 http://www.ncbi.nlm.nih.gov/pubmed/12824330 (accessed January 10, 2018).
[46] Gromacs, A versatile package to perform molecular dynamics, http://www.gromacs.org accessed May 7, 2018.
[47] H. Hernández, C.V. Robinson, Determining the stoichiometry and interactions of macromolecular assemblies from mass spectrometry, Nat. Protoc. 2 (2007) 715–726, https://doi.org/10.1038/nprot.2007.73.
[48] B.T. Ruotolo, J.L.P. Benesch, A.M. Sandercock, S.-J. Hyung, C.V. Robinson, Ion mobility–mass spectrometry analysis of large protein complexes, Nat. Protoc. 3 (2008) 1139–1152, https://doi.org/10.1038/nprot.2008.78.
[49] M.F. Bush, Z. Hall, K. Giles, J. Hoyes, C.V. Robinson, B.T. Ruotolo, Collision cross sections of proteins and their complexes: a calibration framework and database for gas-phase structural biology, Anal. Chem. 82 (2010) 9557–9565, https://doi.org/10.1021/ac1022953.
[50] R. Salbo, M.F. Bush, H. Naver, I. Campuzano, C.V. Robinson, I. Pettersson, T.J.D. Jørgensen, K.F. Haselmann, Travelling-wave ion mobility mass spectrometry of protein complexes: accurate calibrated collision cross-sections of human insulin oligomers, Rapid Commun. Mass Spectrom. 26 (2012) 1181–1193, https://doi.org/10.1002/rcm.6211.
[51] E.G. Marklund, M.T. Degiacomi, C.V. Robinson, A.J. Baldwin, J.L.P. Benesch, Collision cross sections for structural proteomics, Structure 23 (2015) 791–799, https://doi.org/10.1016/j.str.2015.02.010.
[52] J.L. Benesch, B.T. Ruotolo, Mass spectrometry: come of age for structural and dynamical biology, Curr. Opin. Struct. Biol. 21 (2011) 641–649, https://doi.org/10.1016/j.sbi.2011.08.002.
[53] L. Han, B.T. Ruotolo, Ion mobility-mass spectrometry differentiates protein quaternary structures formed in solution and in electrospray droplets, Anal. Chem. 87 (2015) 6808–6813, https://doi.org/10.1021/acs.analchem.5b01010.
[54] G.G. Goss, S. Adamia, F. Galvez, Peanut lectin binds to a subpopulation of mitochondria-rich cells in the rainbow trout gill epithelium, Am. J. Physiol. Regul. Integr. Comp. Physiol. 281 (2001) R1718–R1725 http://www.ncbi.nlm.nih.gov/pubmed/11641145 (accessed November 4, 2015).
[55] Y. Li, Q. Wang, S. Chen, P.H. Brown, R. a Mariuzza, Structure of NKp65 bound to its keratinocyte ligand reveals basis for genetically linked recognition in natural killer gene complex, Proc. Natl. Acad. Sci. U. S. A. 110 (2013) 11505–11510, https://doi.org/10.1073/pnas.1303300110.
[56] R. Berry, N. Ng, P.M. Saunders, J.P. Vivian, J. Lin, F.A. Deuss, A.J. Corbett, C.A. Forbes, J.M. Widjaja, L.C. Sullivan, A.D. McAlister, M.A. Perugini, M.J. Call, A.A. Scalzo, M.A. Degli-Esposti, J.D. Coudert, T. Beddoe, A.G. Brooks, J. Rossjohn, Targeting of a natural killer cell receptor family by a viral immunoevasin, Nat. Immunol. 14 (2013) 699–705, https://doi.org/10.1038/ni.2605.
[57] D. Rozbesky, Z. Sovova, J. Marcoux, P. Man, R. Ettrich, C.V. Robinson, P. Novak, Structural Model of Lymphocyte Receptor NKR-P1C Revealed by Mass Spectrometry and Molecular Modeling, Anal. Chem. 85 (2013) 1597–1604 10.1021/ac302860m.
[58] B.T. Ruotolo, J.L.P. Benesch, A.M. Sandercock, S.-J. Hyung, C.V. Robinson, Ion mobility–mass spectrometry analysis of large protein complexes, Nat. Protoc. 3 (2008) 1139–1152, https://doi.org/10.1038/nprot.2008.78.
[59] L. Kveberg, K.-Z. Dai, M. Inngjerdingen, C.G. Brooks, S. Fossum, J.T. Vaage, Phylogenetic and functional conservation of the NKR-P1F and NKR-P1G receptors in rat and mouse, Immunogenetics. 63 (2011) 429–436, https://doi.org/10.1007/s00251-011-0520-1.